

# Effects of ghost dark energy perturbations on the evolution of spherical overdensities

Mohammad Malekjani<sup>1</sup> <sup>\*</sup>, Tayebe Naderi<sup>1</sup> and Francesco Pace<sup>2</sup>

<sup>1</sup> *Department of Physics, Bu-Ali Sina University, Hamedan 65178, Iran.*

<sup>2</sup> *Jodrell Bank Centre for Astrophysics, School of Physics and Astronomy, The University of Manchester, Manchester, M13 9PL, U.K.*

Accepted ?, Received ?; in original form August 15, 2021

## ABSTRACT

While in the standard cosmological model the accelerated expansion of the Universe is explained by invoking the presence of the cosmological constant term, it is still unclear the true origin of this stunning observational fact. It is therefore interesting to explore alternatives to the simplest scenario, in particular by assuming a more general framework where the fluid responsible of the accelerated expansion is characterised by a time-dependant equation of state. Usually these models, dubbed dark energy models, are purely phenomenological, but in this work we concentrate on a theoretically justified model, the ghost dark energy model. Within the framework of the spherical collapse model, we evaluate effects of dark energy perturbations both at the linear and non-linear level and transfer these results into an observable quantity, the mass function, by speculatively taking into account contributions of dark energy to the mass of the halos. We showed that the growth rate is higher in ghost models and that perturbations enhance the number of structures with respect to the  $\Lambda$ CDM model, with stronger effects when the total mass takes into account dark energy clumps.

## 1 INTRODUCTION

In the standard cosmological model, the small initial fluctuations that were seeded during the phase of inflationary expansion, some  $10^{-35}$  seconds after the Big Bang, are the origin of the large scale structures that we observe today, i.e., galaxies and clusters of galaxies (Starobinsky 1980; H.Guth 1981; Linde 1990). Subsequently these fluctuations grew under the influence of gravitational collapse (Gunn & Gott 1972; Press & Schechter 1974; White & Rees 1978; Peebles 1993; Sheth & Tormen 1999; Peacock 1999; Barkana & Loeb 2001; Peebles & Ratra 2003; Ciardi & Ferrara 2005; Bromm & Yoshida 2011). Most of the growth has taken place after the decoupling of photons and electrons. The spherical collapse model (SCM) introduced by Gunn & Gott (1972) is a simple analytical model to study the evolution of the growth of cosmic structures. The scales of interest in the SCM are much smaller than the Hubble length and the velocities are non-relativistic. Therefore, pseudo-Newtonian gravity can be used to study the evolution of the overdensities. With pseudo-Newtonian gravity we refer to the fact that it is possible to use Newton's hydrodynamical equations in an expanding Universe including relativistic contributions to the Poisson equation, i.e. the contribution of pressure terms. At early times, when the overdensities are small, linear theory is able to follow the evolution of spherical overdense regions. In this phase, due to self gravity, the overdense region expands at a slower rate compared to the Hubble flow. At a particular scale factor, depending on the particular background history, the spherical region reaches a maximum radius and completely detaches from the background expansion. This is the so called turn-around epoch. Subsequently the collapse proceeds under the overdense region own gravity and the system reaches a final steady state with a specific radius due to virialization

processes. The dynamics of the SCM depends strongly on the evolution of the background Hubble flow. The SCM was extended and improved in several works (Fillmore & Goldreich 1984; Bertschinger 1985; Hoffman & Shaham 1985; Ryden & Gunn 1987; Avila-Reese et al. 1998; Subramanian et al. 2000; Ascasibar et al. 2004; Williams et al. 2004). More recently, this formalism has been extended to include shear and rotation terms (del Popolo et al. 2013a,b,c) and non-minimally coupled models (Pace et al. 2014).

On the other hand, recent developments in observational cosmology using high quality data including Type Ia supernovae (SNe Ia), cosmic microwave background (CMB), baryonic acoustic oscillations (BAO) and Large Scale Structure (LSS), converge to a standard cosmological model in a spatially flat geometry with a cosmic dark sector usually in the form of pressureless cold dark matter (CDM) and dark energy (DE) with negative pressure, respectively, in order to interpret the observed flat rotation curves of spiral galaxies and the accelerated expansion of the Universe (Riess et al. 1998; Perlmutter et al. 1999; Jaffe et al. 2001; Riess et al. 2004; Tegmark et al. 2004; Eisenstein et al. 2005; Riess et al. 2007; Ho et al. 2008; Percival et al. 2010; Jarosik et al. 2011; Komatsu et al. 2011; Ade et al. 2013a,b). On the basis of the Planck experiment results (Ade et al. 2013a,b), DE amounts to  $\sim 68\%$ , CDM and usual baryons to  $\sim 27\%$  and  $\sim 5\%$  of the total energy budget of the Universe, respectively.

Einstein's cosmological constant  $\Lambda$  with time independent Equation-of-State (EoS) parameter  $w_\Lambda = -1$  is the first and simplest candidate to describe DE. Although  $\Lambda$  is the simplest model, it suffers from severe theoretical and conceptual problems: the fine-tuning and the cosmic coincidence problems (Sahni & Starobinsky 2000; Weinberg 1989; Carroll 2001;

Peebles & Ratra 2003; Padmanabhan 2003; Copeland et al. 2006). Moreover since  $\Lambda$  is constant in space and time, it does not cluster and has a negligible contribution to the energy density budget of the Universe at high redshifts, so that it affects the evolution of structures in the Universe at  $z \lesssim 1$ .

In order to solve or at least alleviate the theoretical problems of the  $\Lambda$ CDM Universe, a wealth of dynamical DE models with a time varying equation-of-state (EoS) parameter  $w_{\text{de}}(z)$  has been proposed. Scalar fields models including quintessence (Wetterich 1988), phantom (Caldwell 2002; Nojiri & Odintsov 2003a,b), k-essence (Armendariz-Picon et al. 2001; Chiba et al. 2000), tachyon (Sen 2002; Padmanabhan 2002) and dilaton (Gasperini & Veneziano 2002; Arkani-Hamed et al. 2004; Piazza & Tsujikawa 2004) are few examples of such dynamical DE models which have been discussed extensively in literature.

Other dynamical DE models which can successfully interpret the current accelerating Universe are constructed on the basis of quantum gravity theories. Models such as holographic dark energy (HDE) models (Hořava & Minic 2000; Thomas 2002) and agegraphic dark energy (ADE) models (Cai 2007) are derived in the framework of quantum gravity, by introducing a new degree of freedom or by modifying the theory of gravity (Hořava & Minic 2000; Thomas 2002; Cai 2007). Recently, ghost dark energy models have attracted a lot of interests in the category of dynamical DE models (see section 2 for a in depth description of this class of models).

Dynamical DE models not only alleviate the theoretical problems affecting the cosmological constant  $\Lambda$ , but also, like pressureless matter, possess fluctuations. Hence these models directly affect:

- i) the dynamics of the background cosmology through the modification of the Hubble parameter,
- ii) the matter power spectrum and large scale clustering via their fluctuations.

Two parameters are important and give a significant influence to DE perturbations on the matter power spectrum and large scale structure formation. The first is that the EoS parameter of DE should be different from  $-1$ . The second is the effective sound speed  $c_e^2$  which connects the density and pressure perturbations according to  $\delta p = c_e^2 \delta \rho$ . In fact, the sound horizon of DE is given by  $c_s H^{-1}$ . DE can cluster only on scales larger than the sound horizon and smaller than the gravitational horizon,  $c_e H^{-1} < \lambda < H^{-1}$ . Here we consider two different cases (in units of the speed of light,  $c$ ) usually discussed in literature:  $c_e^2 = 1$  (smooth DE) and  $c_e^2 = 0$  (clustering DE). In the first case, the sound horizon of DE is equal to the Hubble length, so that DE perturbations occur on scales equal to or larger than the Hubble horizon and are therefore negligible on sub-Hubble scales. In the second scenario, the sound speed is very small compared to the speed of light  $c$ . Therefore the sound horizon of DE is significantly smaller than the Hubble horizon. In this case one can consider DE perturbations with a wavelength larger than the sound horizon and smaller than the gravitational Hubble horizon which can grow in a similar fashion to matter perturbations which growth under gravitational instability (Abramo et al. 2009; Appleby et al. 2013; Pace et al. 2014; Mehrabi et al. 2014).

The SCM has been investigated and improved in clustering DE models in order to study how DE perturbations impact structure formation in the highly non-linear regime (Abramo et al. 2007, 2009; Pace et al. 2014). In this work we extend the SCM in ghost DE models by taking into account the perturbations of the DE fluid. We study the evolution of overdensities in ghost DE models and obtain the linear overdensity threshold for collapse  $\delta_c$  as well as the

virial overdensity  $\Delta_{\text{vir}}$  parameters. We show how these quantities are affected by DE clustering in ghost DE models. We then follow the SCM in clustering ghost DE Universes by calculating the mass function and the cluster number count with the Press-Schechter formalism.

The paper is organized as following. In section 2 we introduce the ghost DE models and describe the evolution of background cosmology in these models. In section 3 the non-linear SCM in clustering ghost DE models is presented. In section 4 we compute the predicted mass function and cluster number count in ghost DE models using the Press-Schechter formalism by taking into account the clustering DE sector. Finally we conclude and summarise our results in section 5.

## 2 BACKGROUND COSMOLOGY IN GHOST DARK ENERGY MODELS

The origin of ghost fields traces back to Veneziano ghosts which have been proposed to find a solution to the  $U(1)$  problem in the low energy effective QCD theory (Veneziano 1979; Witten 1979; Kawarabayashi & Ohta 1980; Rosenzweig et al. 1980). Although in this formalism the ghost field has no contribution in the flat Minkowski spacetime, in curved spacetime it has a small energy density proportional to  $\Lambda_{\text{QCD}}^3 H$ , where  $H$  is the Hubble parameter and  $\Lambda_{\text{QCD}}^3$  is the QCD mass scale (Ohta 2011). With  $\Lambda_{\text{QCD}}^3 \sim 100 \text{ MeV}$  and  $H \sim 10^{-33} \text{ eV}$ , the quantity  $\Lambda_{\text{QCD}}^3 H$  gives the right order of magnitude of the observed energy density of DE ( $\sim 3 \times 10^{-3} \text{ eV}$ )<sup>4</sup> (Ohta 2011). This small vacuum energy density can be considered as a driver engine for the evolution of the Universe. Comparing with other theoretical dynamical DE models like HDE and ADE models in which one should introduce a new parameter or a new degree of freedom, the most important advantage of ghost DE models is that they come from the standard model of particle physics and are totally embedded both in the standard model and in general relativity without introducing any new parameter or new degrees of freedom. This numerical coincidence also shows that this model can solve the fine tuning problem (Urban & Zhitnitsky 2009a,b, 2010a,b). As it was mentioned above, the energy density in ghost DE model is proportional to the Hubble parameter (Ohta 2011):

$$\rho_{\text{de}} = \alpha H, \quad (1)$$

where  $\alpha > 0$  is roughly of order  $\Lambda_{\text{QCD}}^3$ . From the observational point of view, ghost DE models can fit a whole set of cosmological data including SNe Ia, BAO, CMB, Big Bang nucleosynthesis (BBN) and Hubble parameter data (Cai et al. 2011). The cosmological evolution of the models has been investigated in (Urban & Zhitnitsky 2009a,b, 2010a,b) who stated that the Universe begins to accelerate at redshift around  $z \sim 0.6$ .

The Friedmann equation for a Universe containing pressureless dust matter and DE in a flat geometry described by a Friedmann-Robertson-Walker (FRW) metric is given by

$$H^2 = \frac{8\pi G}{3}(\rho_m + \rho_{\text{de}}), \quad (2)$$

where  $\rho_m$  and  $\rho_{\text{de}}$  are the energy density of the pressureless dust matter and DE components, respectively, and  $H$  is the Hubble parameter. We use equation (1) for the energy density of the DE component and insert it into equation (2) in order to obtain the Hubble

parameter in ghost DE cosmologies

$$H = \frac{4\pi G}{3}\alpha + \sqrt{\left(\frac{4\pi G}{3}\alpha\right)^2 + \frac{8\pi G}{3}\rho_{m0}a^{-3}}. \quad (3)$$

In terms of the dimensionless energy density  $\Omega_{m,0} = 8\pi G\rho_{m,0}/(3H_0^2)$  and redshift parameter  $z = 1/a - 1$ , the above Hubble equation becomes

$$H(z) = H_0 \left( \kappa + \sqrt{\kappa^2 + \Omega_{m,0}(1+z)^3} \right), \quad (4)$$

where  $\kappa = (1 - \Omega_{m,0})/2$ .

In the above mentioned studies, the energy density of ghost DE is assumed to be proportional to the Hubble parameter via equation (1). However, the energy density of the Veneziano ghost field in QCD theory is generally of the form  $H + O(H^2)$  (Zhitnitsky 2011). Although in ghost DE models only the leading term  $H$  was assumed, it has been shown that the sub-leading term  $H^2$  can also be important in the early evolution of the Universe (Maggiore et al. 2012). A ghost DE model with sub-leading term  $H^2$  is usually called generalised ghost dark energy model. Cai et al. (2012) showed that generalised ghost DE models result in better agreement with observations compared to ordinary ghost DE models. The energy density of a generalised ghost DE model is given by (Cai et al. 2011)

$$\rho_{de} = \alpha H + \beta H^2, \quad (5)$$

where  $\alpha$  and  $\beta$  are the constants of the model. Inserting equation (5) into equation (2), the Hubble parameter becomes

$$H = \frac{4\pi G}{3\gamma}\alpha + \sqrt{\left(\frac{4\pi G}{3\gamma}\alpha\right)^2 + \frac{8\pi G}{3\gamma}\rho_{m0}a^{-3}}, \quad (6)$$

where  $\gamma = 1 - 8\pi G\beta/3$ . Setting  $\gamma = 1$ , generalised ghost DE model reduces to ordinary ghost DE model ( $\beta = 0$ ), as expected. In terms of the dimensionless matter energy density  $\Omega_{m,0}$  and redshift parameter  $z$ , the Hubble equation in generalised ghost DE models is given by

$$H(z) = H_0 \left( \kappa + \sqrt{\kappa^2 + \frac{\Omega_{m,0}(1+z)^3}{\gamma}} \right), \quad (7)$$

where  $\kappa = (1 - \Omega_{m,0}/\gamma)/2$ .

The conservation equations for pressureless dust matter and DE at the background level are

$$\dot{\rho}_m + 3H\rho_m = 0, \quad (8)$$

$$\dot{\rho}_{de} + 3H(1 + w_{de})\rho_{de} = 0, \quad (9)$$

where the dot is the derivative with respect to cosmic time and  $w_{de}$  is the DE EoS parameter.

Taking the time derivative of Friedmann equation (2) and using equations (8) and (9) as well as the critical density  $\rho_c = 3H^2/(8\pi G)$ , we obtain

$$\frac{\dot{H}}{H^2} = -\frac{3}{2}(1 + \Omega_{de}w_{de}), \quad (10)$$

where  $\Omega_{de}$  is the dimensionless density parameter of the DE component. Differentiating equations (1) and (5) with respect to time and inserting the results in the conservation equation for DE (equation 9) and also using equation (10), the EoS parameter for ghost DE and generalised ghost DE models are

$$w_{de}(z) = \frac{1}{\Omega_{de}(z) - 2}, \quad (11)$$

$$w_{de}(z) = \frac{1 - \Omega_{de}(z) - \gamma}{\Omega_{de}(z)(1 - \Omega_{de}(z) + \gamma)}. \quad (12)$$

Setting  $\gamma = 1$ , equation (12) reduces to (11) as expected. We now calculate the equation of motion for the energy density of DE in ghost DE and generalised ghost DE models. Taking the time derivative of  $\Omega_{de} = \rho_{de}/\rho_c$  and using equations (1) and (10) and finally changing the time derivative to a derivative with respect to cosmic redshift  $z$ , we have

$$\frac{d\Omega_{de}(z)}{dz} = -\frac{3\Omega_{de}(z)}{2(1+z)} [1 + \Omega_{de}(z)w_{de}(z)], \quad (13)$$

for both ghost and generalised ghost DE cosmologies. We see that the evolution of the DE density in ghost DE cosmologies via equation (13) depends on the EoS parameter of the models according to the relations (11) and (12). We solve the system of coupled equations (4), (11), (13) and (7), (12), (13) in order to calculate the evolution of the Hubble and EoS parameters as well as the energy density of DE in ghost and generalised ghost DE cosmologies, respectively. To fix the cosmology, the present values of matter density and DE density parameters are chosen as:  $\Omega_{m,0} = 0.27$  and  $\Omega_{de,0} = 0.73$  in a spatially flat Universe. The present Hubble parameter is  $H_0 = 70$  km/s/Mpc.

In figure (1) we show the evolution of the EoS parameter  $w_{de}$  (top panel), dimensionless Hubble parameter  $E = H/H_0$  (middle panel) and energy density of DE component  $\Omega_{de}$  (bottom panel) as a function of the cosmic redshift  $z$  for different ghost, generalised ghost DE and  $\Lambda$ CDM cosmological models. In the case of the generalised ghost DE model we choose the model parameter  $\gamma$  as 0.96 and 0.90. In all the figures of this work we indicate the ghost DE as GDE and the generalised ghost DE as GGDE. We see that the EoS parameter for ghost and generalised ghost DE models is always bigger than  $w_\Lambda = -1$  and remains in the quintessence regime, i.e.,  $w_{de} > -1$ . The Hubble parameter and the DE density are bigger in these models compared to the concordance  $\Lambda$ CDM Universe. This means that the rate of acceleration is stronger for (generalised) ghost models and that the relevance of the DE fluid is important for a longer period of the cosmic history.

### 3 SPHERICAL COLLAPSE IN GHOST DARK ENERGY COSMOLOGIES

In this section we investigate the SCM in the framework of clustering ghost and generalised ghost DE cosmologies. The effects of DE perturbations on the evolution of matter overdensities have been extensively investigated in literature (see, i.e. Mota & van de Bruck 2004; Abramo et al. 2007, 2008, 2009; Creminelli et al. 2010; Basse et al. 2011; Batista & Pace 2013; Pace et al. 2014). Following Pace et al. (2014), the fully perturbed equations for the evolution of non-relativistic dust matter  $\delta_m$  and dark energy  $\delta_{de}$  perturbations in the non-linear regime (without the contribution of shear and rotation) are given by

$$\delta'_m + (1 + \delta_m) \frac{\tilde{\theta}}{a} = 0 \quad (14)$$

$$\delta'_{de} - \frac{3}{a}w_{de}\delta_{de} + [1 + w_{de} + \delta_{de}] \frac{\tilde{\theta}}{a} = 0 \quad (15)$$

$$\tilde{\theta}' + \left( \frac{2}{a} + \frac{E'}{E} \right) \tilde{\theta} + \frac{\tilde{\theta}^2}{3a} + \frac{3}{2a} [\Omega_{DM}\delta_m + \Omega_{de}\delta_{de}] = 0 \quad (16)$$

where  $\tilde{\theta} = \theta/H$  is the dimensionless divergence of the comoving peculiar velocity for dust matter and DE.

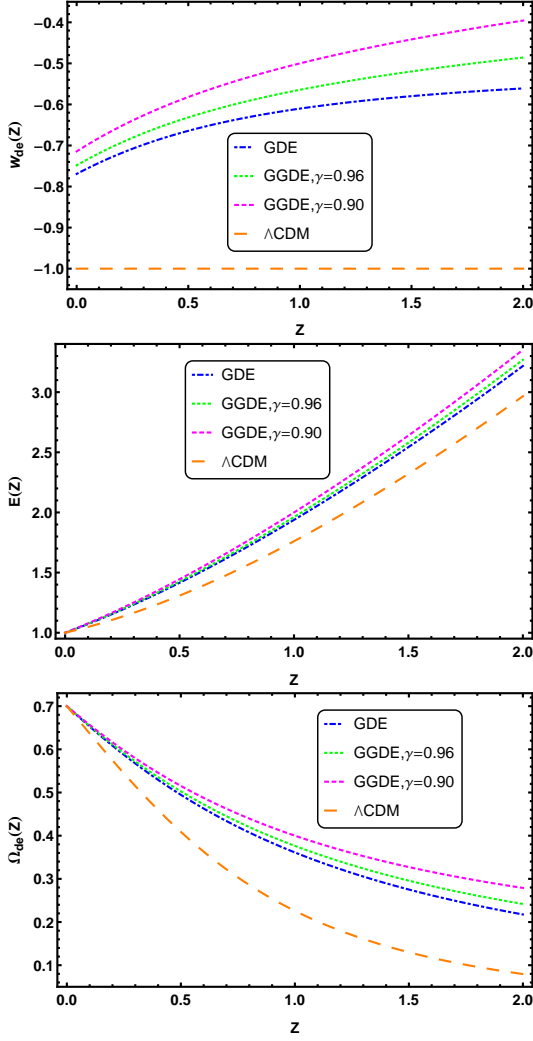


**Figure 1.** Top panel: Evolution of the EoS parameter  $w_{\text{de}}$ . Middle panel: dimensionless Hubble parameter  $E(z)$ . Bottom panel: DE density parameter  $\Omega_{\text{de}}$  as a function of cosmic redshift  $z$  for the different cosmological models considered in this work. As shown in the legend, the ghost DE is indicated by GDE, generalised ghost DE by GGDE. The  $\Lambda$ CDM model is shown with the orange dashed line, the GDE model with the red short-short dashed line and the GGDE model with the brown (pink) short-dashed line for  $\gamma = 0.96$  ( $\gamma = 0.90$ ), respectively.

The linear evolution of overdensities at early times is

$$\delta'_m + \frac{\tilde{\theta}}{a} = 0, \quad (17)$$

$$\delta'_{\text{de}} - \frac{3}{a} w_{\text{de}} \delta_{\text{de}} + [1 + w_{\text{de}}] \frac{\tilde{\theta}}{a} = 0, \quad (18)$$

$$\tilde{\theta}' + \left( \frac{2}{a} + \frac{E'}{E} \right) \tilde{\theta} + \frac{3}{2a} [\Omega_{\text{DM}} \delta_m + \Omega_{\text{de}} \delta_{\text{de}}] = 0 \quad (19)$$

As in Pace et al. (2014), to determine the initial conditions to solve the above differential equations describing the evolution of perturbations, we find the initial value  $\delta_{\text{m},i}$  such that at the collapse scale factor  $a_c$  the matter overdensity diverges,  $\delta_m \rightarrow \infty$ . The initial values for the DE overdensity  $\delta_{\text{de},i}$  and peculiar velocity perturbation  $\tilde{\theta}_i$  are related to  $\delta_{\text{m},i}$  via (Batista & Pace 2013; Pace et al.

2014):

$$\delta_{\text{de},i} = \frac{n}{(n-3w)} (1 + w_{\text{de}}) \delta_{\text{m},i}, \quad (20)$$

$$\tilde{\theta}_i = -n \delta_{\text{m},i}. \quad (21)$$

In the case of an EdS model  $n = 1$ . However, in DE cosmologies it has been shown that there is a small deviation from unity (Batista & Pace 2013). In the limiting case of non-clustering DE models ( $c_e = 1$ ) the coupled non-linear equations (14, 15, 16) and system of linear equations (17, 18, 19), respectively, reduce to the following equations:

$$\delta''_m + \left( \frac{3}{a} + \frac{E'}{E} \right) \delta'_m - \frac{4}{3} \frac{\delta_m'^2}{1 + \delta_m} - \frac{3\Omega_{m0}}{2a^5 E^2} \delta_m (1 + \delta_m) = 0, \quad (22)$$

$$\delta''_m + \left( \frac{3}{a} + \frac{E'}{E} \right) \delta'_m - \frac{3\Omega_{m0}}{2a^5 E^2} \delta_m = 0, \quad (23)$$

as expected (see also Pace et al. 2010). In the case of non-clustering ghost and generalised ghost DE models, we will solve equations (22, 23), instead of the previous ones.

## 4 RESULTS

We first solve the system of equations (17), (18), (19) for the case of clustering DE ( $c_e = 0$ ) and (23) for non-clustering DE ( $c_e = 1$ ) in order to determine the linear evolution of the overdensities  $\delta_m$  and  $\delta_{\text{de}}$  ( $\delta_m$  in the non-clustering DE case) and obtain the linear growth factor  $D_+(z) = \delta_m(z)/\delta_m(z=0)$  as a function of cosmic redshift  $z$  for the different cosmological models considered in this work.

In figure (2), the evolution of the growth factor normalised at  $z = 0$  and divided by the scale factor  $a$  is presented as a function of redshift. In the EdS model (black solid line)  $D_+/a$  is equal to 1 at any time showing that the growth of matter perturbations  $\delta_m$  is the same at all redshifts. In a  $\Lambda$ CDM Universe (orange long-dashed curve) the growth factor is higher than the EdS model throughout its history, but falls for lower redshifts. The lowering of the growth factor at lower redshifts is due to the fact that at late times the cosmological constant dominates the energy budget of the Universe and suppresses the amplitude of perturbations. On the other hand, a larger growth factor in a  $\Lambda$ CDM Universe at higher redshift shows that the growth of dust matter perturbations will be stronger than in a EdS Universe at early times. For ghost and generalised ghost DE models we show  $D_+/a$  for two extreme cases: fully clustering DE ( $c_e = 0$ ) and homogeneous DE ( $c_e = 1$ ) models. In the case of generalised ghost DE model, we choose a value of 0.96 for the model parameter  $\gamma$ . The red and brown dashed curves stand for clustering ghost and generalised ghost DE models, respectively. The blue dotted-dashed and green dotted curves show the variation of  $D_+/a$  for homogeneous ghost and generalised ghost DE Universes, respectively. We see that the growth factor is largest (intermediate) for homogeneous (clustering) ghost and generalised ghost DE models compared to the concordance  $\Lambda$ CDM Universe. It is worth to mention that  $D_+/a$  changes more rapidly at low redshifts where dark energy dominates the energy budget of the Universe. At early times instead, the relative change is much shallower. Differences are obviously still noticeable in the models. In particular we notice that while  $D_+/a$  for the  $\Lambda$ CDM model is almost a constant, this is not entirely the case for the dark energy models analysed in this work. This is easily interpreted taking into account the stronger importance of dark energy at early times, as clearly shown in the lower panel of figure (1). Similarly to the



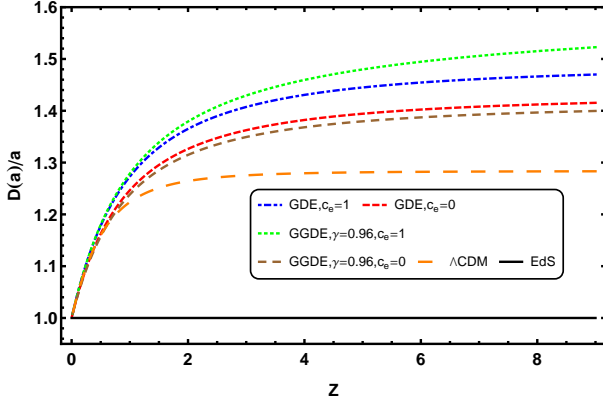


**Figure 2.** Time evolution of the growth factor normalised to the present time and divided by the scale factor  $a$  as a function of the cosmic redshift  $z$  for different cosmological models. Black solid line shows the EdS model, the orange long-dashed line the  $\Lambda$ CDM model, the blue (green) dot-dashed (dotted) line the homogeneous ghost (generalised ghost) DE model, while the red (brown) dashed line the clustering ghost (generalised ghost) DE cosmology.

$\Lambda$ CDM Universe, in ghost and generalised ghost DE models, DE suppresses the growth of perturbations at low redshifts. More quantitatively, at high redshifts, the growth of perturbations parameter  $D_+/a$  in non-clustering (clustering) generalised ghost DE model is  $\approx 18.7\%$  ( $\approx 10.9\%$ ) larger than in the  $\Lambda$ CDM concordance model. These values are only mildly larger than the ghost dark energy models, where  $D_+/a$  differs of  $\approx 14.5\%$  ( $\approx 10\%$ ) for non-clustering (clustering) ghost DE models with respect to a  $\Lambda$ CDM model.

#### 4.1 Spherical Collapse Model parameters

Here we evaluate the two characterising quantities of the spherical collapse model: the linear overdensity parameter  $\delta_c$  and the virial overdensity  $\Delta_{\text{vir}}$  for ghost and generalised ghost DE cosmologies. The linear overdensity  $\delta_c$  together with the growth factor  $D_+$  is important in order to evaluate the mass function in the Press Schechter formalism (Press & Schechter 1974; Bond et al. 1991; Sheth & Tormen 2002). The virial overdensity  $\Delta_{\text{vir}}$  is used to calculate the size of spherically symmetric halos with given mass  $M$ .

We search the initial conditions  $\delta_{m,i}$  following the general approach in Pace et al. (2010, 2012) and then we use equations (20) and (21) to determine  $\delta_{\text{de},i}$  and  $\theta_i$ . Once the initial conditions are found, we then solve the system of equations (17), (18) and (19) in order to obtain  $\delta_c = \delta_m(z = z_c)$ . In the non-clustering case, we solve equation (23) to calculate  $\delta_c$ .

The collapse redshift  $z_c$  is defined as the redshift at which the matter overdensity tends to infinity  $\delta_m \rightarrow \infty$  (see also Pace et al. 2010, 2012, 2014).

In figure (3) the evolution of the linear overdensity  $\delta_c$  as a function of the collapse redshift  $z_c$  is presented for different models: EdS,  $\Lambda$ CDM, homogeneous and clustering ghost DE and clustering generalised ghost DE. We refer to the caption for line styles and colours of each model. Analogously to the previous section, we use  $\gamma = 0.96$  in the case of generalised ghost DE models. In all DE models, the linear overdensity parameter approaches the fiducial value in the EdS Universe  $\delta_c \approx 1.686$  at high enough redshifts, as expected. In fact at high redshifts, the Universe is dominated by pressureless dust matter and the effects of DE on the scenario of structure formation is negligible. At lower redshifts,  $\delta_c$  de-

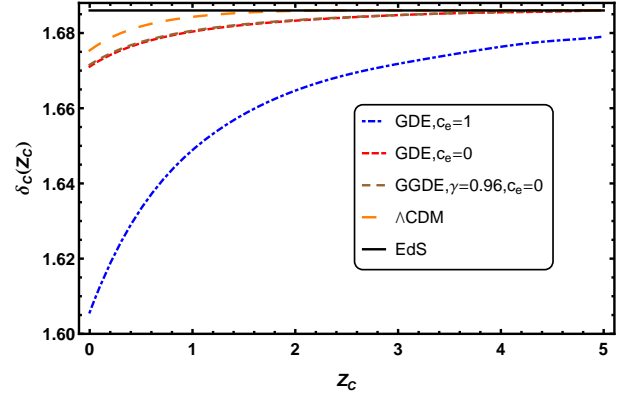


**Figure 3.** The variation of the linear threshold density contrast  $\delta_c$  as a function of the collapse redshift for the different cosmological models analysed in this work. Line styles and colours are as in Fig. 2.

creases and deviates from the EdS limit. The important point to note is that in clustering ghost and generalised ghost DE models, the behaviour of  $\delta_c$  is more similar to the  $\Lambda$ CDM Universe with respect to the homogeneous models. This result is in agreement with what found by Pace et al. (2010) and Batista & Pace (2013) for early dark energy models and Pace et al. (2014) for clustering quintessence and phantom DE models. Quantitatively we see that the differences between homogeneous ghost and generalised ghost DE models with the  $\Lambda$ CDM model at the present time are roughly 4.5% and 21.5%, respectively, while in the case of clustering ghost and generalised ghost models the differences are very small, of the order of  $\approx 0.25\%$  for both cases. As for the case of perturbations in early dark energy models, we can explain the fact that perturbations in the dark energy fluid make the model more similar to the  $\Lambda$ CDM model by taking into account that the Poisson equation is now modified and the gravitational potential is sourced also by DE perturbations.

In the framework of the SCM, the virialization process of pressureless dust matter and the size of forming halos are strongly affected by the DE sector (Lahav et al. 1991; Wang & Steinhardt 1998; Mota & van de Bruck 2004; Horellou & Berge 2005; Wang & Tegmark 2005) and also its perturbations (Abramo et al. 2007, 2008, 2009; Batista & Pace 2013; Pace et al. 2014). The virial overdensity is defined as  $\Delta_{\text{vir}} = \zeta(x/y)^3$ , where  $\zeta$  is the overdensity at the turn-around epoch,  $x$  is the scale factor normalised to the turn-around scale factor and  $y$  is the ratio between the virialization radius and the turn-around radius (Wang & Steinhardt 1998). In an EdS cosmology, it is simple to show that  $y = 1/2$ ,  $\zeta \approx 5.6$  and  $\Delta_{\text{vir}} \approx 178$  independently of the cosmic redshift (see also Naderi et al. 2015). In DE cosmologies,  $\Delta_{\text{vir}}$  depends on the evolution of the DE fluid and it is a redshift dependent quantity. In particular, according to whether DE takes part or not into the virialization process, the quantity  $y$  may be larger or smaller than  $1/2$  and the parameter  $\Delta_{\text{vir}}$  can be affected by the clustering of DE (Maor & Lahav 2005; Pace et al. 2014).

In the line of these studies, we calculate the turn-around and virial overdensities  $\zeta$  and  $\Delta_{\text{vir}}$  in ghost and generalised ghost DE cosmologies. We also determine how the clustering of the DE component can change the variation of  $\zeta$  and  $\Delta_{\text{vir}}$  in these models. Our results are presented in figure (4). In the top panel, the variation of the overdensity at the turn-around redshift  $\zeta$  is shown for the different DE models investigated in this work. In the limiting case

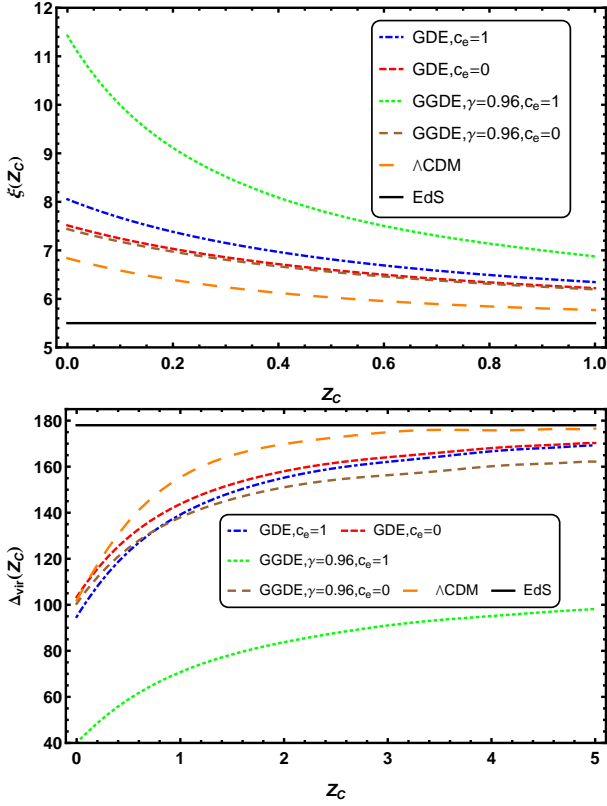


**Figure 4.** The variation of turn around overdensity  $\zeta$  (top panel) and virial overdensity  $\Delta_{\text{vir}}$  (bottom panel) with respect to the collapse redshift  $z_c$  for various models considered in this work. Line styles and colours are as in Fig. 2.

of the EdS model,  $\zeta = 5.6$  independently of the cosmic time. At early times,  $\zeta$  tends to the critical value  $\zeta = 5.6$  representing the early matter-dominated era. The value of  $\zeta$  is larger for both clustering and non-clustering versions of ghost and generalised ghost DE models, compared to the concordance  $\Lambda$ CDM model. Differences between the dark energy models and the  $\Lambda$ CDM model cover a relatively huge spectrum of values, according to whether we take into account the perturbations of the dark energy fluid. In particular for homogeneous (generalised) ghost DE models, differences are of the order of (67%) 17% while when perturbations are taken into account, differences drop down to (9%) 10%. This shows how the generalised ghost model, is much more sensitive to the inclusion of DE perturbations. Once again, this is due the higher amount of DE density at earlier time for these kind of models. Hence we conclude that in the context of ghost DE scenarios the perturbed spherical perturbations detach from the background Hubble flow with higher overdensities compared to the EdS and  $\Lambda$ CDM Universes. We also notice that the results for clustering ghost and generalised ghost DE models are closer to what is found for the reference  $\Lambda$ CDM model compared to the non-clustering case.

In the bottom panel, the results for the virial overdensity  $\Delta_{\text{vir}}$  are presented. In the case of ghost DE models, the results are closer to the reference  $\Lambda$ CDM model. In these models, the difference between homogeneous and clustering DE is very small. However, in the case of generalised ghost cosmology the differences are more pronounced. Differences between ghost DE models and  $\Lambda$ CDM model at the present time are of the order of 60% for non-clustering generalised ghost DE model and 7% for homogenous ghost DE

models, roughly as for the overdensity at the turn-around radius. This is not surprising, since this quantity is the main ingredient used to evaluate the virial overdensity. When perturbations in dark energy are taken into account differences are only of the order of 1.5% for both classes analysed. These results are similar to what found in del Popolo et al. (2013b) and Pace et al. (2014).

## 4.2 Mass function and halo number density

We know that galaxies and cluster of galaxies are embedded in the extended halos of cold dark matter (CDM). In the Press & Schechter formalism (Press & Schechter 1974), the abundance of CDM halos can be described as a function of their mass and a Gaussian distribution function expresses the fraction of the volume of the Universe which collapses into an object of mass  $M$  at a certain redshift  $z$ . In this formalism, the comoving number density of virialised structures with masses in the range of  $M$  and  $M + dM$  at redshift  $z$  is given by

$$\frac{dn(M, z)}{dM} = -\frac{\rho_{m0}}{M} \frac{d \ln \sigma(M, z)}{dM} f(\sigma), \quad (24)$$

where  $\sigma$  is the r.m.s. of the mass fluctuation in spheres of mass  $M$  and  $f(\sigma)$  is the mass function. The standard mass function in the Press & Schechter formalism is given by (Press & Schechter 1974)

$$f(\sigma) = \sqrt{\frac{2}{\pi}} \frac{\delta_c(z)}{\sigma(M, z)} \exp \left[ -\frac{\delta_c^2(z)}{2\sigma^2(M, z)} \right]. \quad (25)$$

Although the standard mass function provides a good general representation of the predicted number density of CDM halos, it deviates from simulations due to an over-prediction of low-mass objects and an under-prediction of high-mass objects at the present time (Sheth & Tormen 1999, 2002). Here we use another popular fitting formula proposed by Sheth & Tormen (Sheth & Tormen 1999, 2002), the so-called ST mass function:

$$f_{\text{ST}}(\sigma) = A \sqrt{\frac{2a}{\pi}} \left[ 1 + \left( \frac{\sigma^2(M, z)}{a\delta_c^2(z)} \right)^p \right] \frac{\delta_c(z)}{\sigma(M, z)} \exp \left( -\frac{a\delta_c^2(z)}{2\sigma^2(M, z)} \right), \quad (26)$$

where the numerical parameters are:  $A = 0.3222$ ,  $a = 0.707$  and  $p = 0.3$ . Putting  $A = 1/2$ ,  $a = 1$  and  $p = 0$ , the well known Press-Schechter mass function can be recovered as expected. In a Gaussian density field, the mass variance  $\sigma^2$  is given by

$$\sigma^2 = \frac{1}{2\pi^2} \int_0^\infty k^2 P(k) W^2(kR) dk, \quad (27)$$

where  $R = (3M/4\pi\rho_{m,0})^{1/3}$  is the radius of the overdense spherical path at the present time,  $W(kR) = 3[\sin(kR) - kR \cos(kR)]/(kR)^3$  is the Fourier transform of a spherical top-hat profile window function with radius  $R$  and  $P(k)$  is the linear power spectrum of density fluctuations (Peebles 1993).

The number density of objects above a given mass at a certain fixed redshift is

$$n(> M) = \int_M^\infty \frac{dn}{dM'} dM'. \quad (28)$$

In this section, having at hands all the necessary ingredients, we can compute the predicted number density of virialised objects in the Press-Schechter formalism for ghost and generalised ghost DE cosmologies. As first step, we use equation (28) for non-clustering ghost and generalised ghost DE models. In next section we investigate the predicted number density of virialised clusters on the basis of the formulation presented in Creminelli et al. (2010);

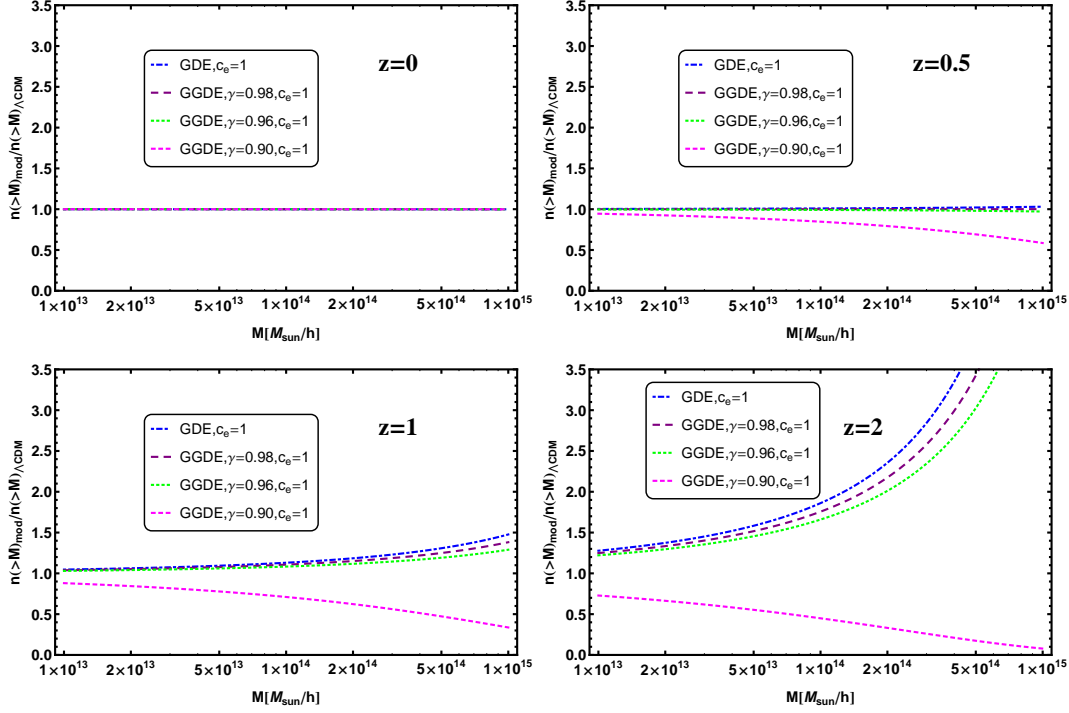


**Figure 5.** Ratio of the number of objects above a given mass  $M$  for halos at  $z = 0$  (top left),  $z = 0.5$  (top right),  $z = 1.0$  (bottom left) and  $z = 2.0$  (bottom right) between the ghost and generalised ghost DE models and the concordance  $\Lambda$ CDM model. The blue dotted-dashed curve represents the ghost DE model. The purple dashed, green dotted and pink dashed curves stand for generalised ghost DE model with model parameter  $\gamma = 0.98$ ,  $\gamma = 0.96$  and  $\gamma = 0.90$ , respectively.

Basse et al. (2011); Batista & Pace (2013) where the total mass of the halos is affected by DE perturbations.

We use the  $f_{ST}$  mass function given in equation (26) and choose four different redshifts:  $z = 0$ ,  $z = 0.5$ ,  $z = 1.0$  and  $z = 2.0$ . In order to calculate  $\sigma^2$ , we follow the formulations presented in Abramo et al. (2007) and Naderi et al. (2015). We also adopt the  $\Lambda$ CDM model as reference model with normalization of the matter power spectrum  $\sigma_8 = 0.776$ , in agreement with recent observations (??). In figure (5), we show the ratio of the number of objects above a given mass  $M$  between the ghost and generalised ghost DE models and the concordance  $\Lambda$ CDM model, in the case of non-clustering DE cosmologies. In the case of generalised ghost DE model, we choose three different values for the model parameter:  $\gamma = 0.90$ ,  $\gamma = 0.96$  and  $\gamma = 0.98$ . As was discussed in section (2), for  $\gamma = 1.0$ , the generalised ghost model reduces to the ghost DE model. In the upper left (right) panel, the results are presented for redshift  $z = 0$  ( $z = 0.5$ ). The lower left (right) panel is for halos at redshift  $z = 1$  ( $z = 2$ ), as indicated in the legends. Due to the identical normalization of the matter power spectrum, we see that at  $z = 0$  all models have the same number of objects. At  $z = 0.5$ , the ghost ( $\gamma = 1$ ) and generalised ghost with  $\gamma = 0.96$  and  $\gamma = 0.98$  are still giving the same number of object compared to the concordance  $\Lambda$ CDM model, with very small differences for the large mass tail of the distribution ( $10^{15} M_\odot/h$ ). However, for smaller values of  $\gamma$  the differences between the generalised ghost and the  $\Lambda$ CDM model are considerable. For  $\gamma = 0.90$ , the predicted number density for virialised halos at high mass tail ( $10^{15} M_\odot/h$ ) is roughly 40% lower than the concordance  $\Lambda$ CDM model (see top-right panel of figure (5)). At higher redshifts,  $z = 1$  and  $z = 2$ , the predicted number of struc-

tures exceeds what predicted by the  $\Lambda$ CDM model, in the cases of ghost and generalised ghost DE models with model parameter  $\gamma$  close to unity, i.e.,  $\gamma = 0.96, 0.98$ . The generalised ghost model with low value  $\gamma = 0.90$  shows a decrement in the number of objects compared to other cases. We see that a major difference between ghost DE models and  $\Lambda$ CDM model takes place at high mass while all models are roughly producing the same number of objects at the low mass tail, as expected. From a more quantitative point of view, at redshift  $z = 1$ , the ghost DE model shows an increment in the number of structures of  $\approx 47\%$ , while for the generalised ghost DE model with  $\gamma = 0.98$  ( $\gamma = 0.96$ ) the increment is  $\approx 38\%$  ( $\approx 29\%$ ), when they are compared to the standard  $\Lambda$ CDM model. Surprisingly, the case with  $\gamma = 0.90$  shows a substantial lack of high mass objects, of the order of  $\approx 66\%$  for objects of mass  $\approx 10^{15} M_\odot/h$ .

### 4.3 Corrected mass function in clustering ghost DE models

It is well known that in EdS cosmology  $y = R_{\text{vir}}/R_{\text{ta}} = 1/2$ . In the EdS model, the virial overdensity can be calculated analytically and the calculations lead to  $\Delta_{\text{vir}} \simeq 178$  independently of the redshift  $z$ . It is also well known that this value strongly depends on the particular background cosmology and changes in the presence of DE. It was shown that the virialization process of dark matter overdensities in the non-linear regime depends on the properties of DE models (Lahav et al. 1991; Maor & Lahav 2005; Creminelli et al. 2010; Basse et al. 2011). Moreover, in clustering DE models, we should take into account the contribution of DE perturbations to the total mass of the halos (Creminelli et al. 2010; Basse et al. 2011; Batista & Pace 2013; Pace et al. 2014). Depend-

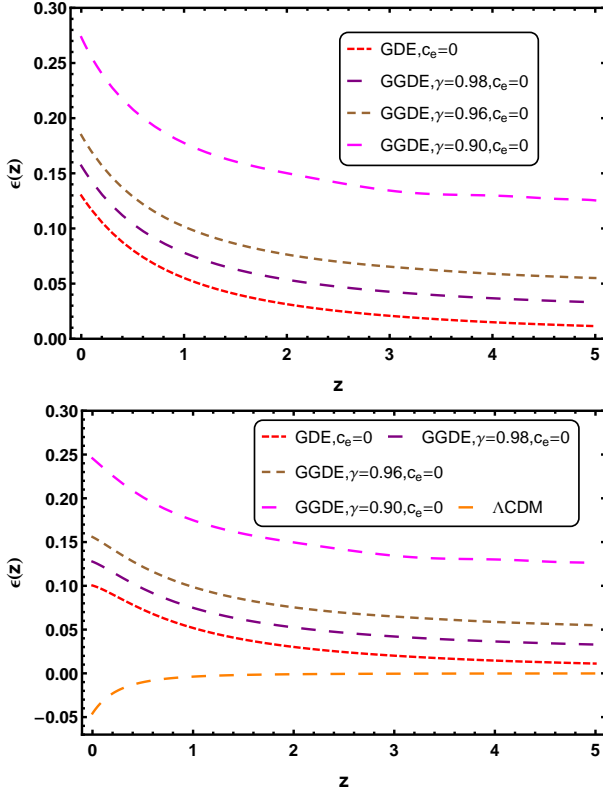


**Figure 6.** The ratio of DE mass to dark matter mass by using the definition of  $\epsilon$  via equation (32) in the top panel and equation (33) in the bottom panel. The red dotted-dashed curve represents the clustering ghost DE model. The purple long dashed, brown dashed and pink long-dashed curves stand for clustering generalised ghost DE model with model parameter  $\gamma = 0.98$ ,  $\gamma = 0.96$  and  $\gamma = 0.90$ , respectively. The orange long dashed one indicates the  $\Lambda$ CDM model.

ing on the quintessence or phantom DE EoS parameter,  $w_{\text{de}}(z)$ , DE can add or subtract mass to the total mass of the halo, respectively. The fraction of DE mass to be taken into account with respect to the mass of the dark matter is given by the quantity  $\epsilon(z) = M_{\text{de}}/M_{\text{m}}$ . The mass of dark matter  $M_{\text{m}}$  is defined as

$$M_{\text{m}} = 4\pi\bar{\rho}_{\text{m}} \int_0^{R_{\text{vir}}} dR R^2 (1 + \delta_{\text{m}}) . \quad (29)$$

where  $\bar{\rho}_{\text{m}}$  is the mean density of dark matter. The mass of DE in the virialization process depends on what it is considered to be the mass of the DE component. If we only assume the contribution of DE perturbation, then the mass of the DE component is given by

$$M_{\text{de}}^{\text{P}} = 4\pi\bar{\rho}_{\text{de}} \int_0^{R_{\text{vir}}} dR R^2 \delta_{\text{de}} (1 + 3c_{\text{e}}^2) , \quad (30)$$

where  $\bar{\rho}_{\text{de}}$  is the mean density of dark energy. On the other hand, if we assume also the contribution at the background level (in analogy to dark matter), the total mass of DE is given by

$$M_{\text{de}}^{\text{T}} = 4\pi\bar{\rho}_{\text{de}} \int_0^{R_{\text{vir}}} dR R^2 [(1 + 3w_{\text{de}}) + \delta_{\text{de}}(1 + 3c_{\text{e}}^2)] . \quad (31)$$

Here we compute the quantity  $\epsilon(z)$  in the case of full clustering DE scenario. It should be noted that due to the background contribution in equation (31), even in the case of homogeneous DE scenarios, DE can add or subtract mass to the dark matter halos (see also Batista & Pace 2013; Pace et al. 2014). Since we work in

the framework of the top-hat spherical profile, the quantities inside the collapsing sphere evolve only in time without any spatial dependency. Hence on the basis of the definition in equation (30) we have

$$\epsilon(z) = \frac{\Omega_{\text{de}}(z)}{\Omega_{\text{m}}(z)} \frac{\delta_{\text{de}}}{1 + \delta_{\text{m}}} , \quad (32)$$

and under the same assumption for equation (31)

$$\epsilon(z) = \frac{\Omega_{\text{de}}(z)}{\Omega_{\text{m}}(z)} \frac{1 + 3w_{\text{de}}(z) + \delta_{\text{de}}}{1 + \delta_{\text{m}}} . \quad (33)$$

In figure (6) we show the evolution of  $\epsilon(z)$  according to equations (32) (top panel) and (33) (bottom panel) for both ghost and generalised ghost DE models. We refer the reader to the caption for line styles and colours. We notice that according to equation (32), both ghost and generalised ghost DE models give a positive contribution to the total mass of the halos ( $\epsilon(z) > 0$ ). The quantity  $\epsilon$  grows with redshift  $z$  meaning that the contribution of DE on the total mass is larger for halos which virialize at lower redshifts. This is explained by taking into account the fact that at late times dark energy perturbations arise, while being negligible at earlier times. In particular, the generalised ghost DE model gives a higher contribution of DE to the total mass of halos compared to ghost DE model. We also see that a lower value of the model parameter  $\gamma$  results in a higher value of  $\epsilon(z)$ . On the other hand, using the definition in equation (33), the behaviour of  $\epsilon$  is different. Looking at equation (33), we see that the sign of the quantity  $1 + 3w_{\text{de}} + \delta_{\text{de}}$  determines how DE contributes to the total mass of the halo. During the history of the halo, when  $3w_{\text{de}} + \delta_{\text{de}} < -1$ , the contribution of the DE mass is negative and therefore it lowers the total mass of the halos. The other important point to note is that according to the definition of  $\epsilon$  via equation (33), one can consider the DE mass even for homogeneous DE models ( $\delta_{\text{de}} = 0$ ). Hence in the bottom panel of figure (6) we show  $\epsilon$  for the  $\Lambda$ CDM model ( $w_{\text{de}} = -1$ ). We also see that for the  $\Lambda$ CDM model  $\epsilon$  is always negative. On the other hand, when  $3w_{\text{de}} + \delta_{\text{de}} > -1$ , the contribution of DE is positive. This is the behaviour taking place for ghost and generalised ghost DE models. Comparing the top and bottom panels in figure (6), we see that for ghost and generalised DE models the values of  $\epsilon$  according to the second definition are lower than equation (32).

We now compute the number density of virialized halos in the presence of DE mass correction. Following the procedure outlined in Batista & Pace (2013) and Pace et al. (2014), in the presence of DE perturbations, we change the mass of halos as  $M \rightarrow M(1 - \epsilon)$ . In this case the corrected mass function can be redefined as follows (Batista & Pace 2013)

$$\frac{dn_{\text{c}}(z, M)}{dM} = -\frac{\rho_{\text{m}0}}{M(1 - \epsilon)} \frac{d \ln \sigma(M, z)}{dM} f(\sigma) , \quad (34)$$

where  $f(\sigma)$  is given by equation (26). It should be noted that the clustering of the DE component can also change the mass function  $f(\sigma)$  by changing the quantities  $\delta_{\text{c}}$  and  $\sigma(M, z)$ . In figure (7) we show the relative number density by using the corrected mass function formula in equation (34) and the definition of  $\epsilon$  in equation (32). Analogously to figure (5), we choose four different redshifts  $z = 0, 0.5, 1$  and  $z = 2$ . We see that due to the contribution of the DE mass, the relative number density between ghost and generalised DE models and  $\Lambda$ CDM model  $n_{\text{c}}/n_{\Lambda\text{CDM}}$  is equal or larger than one. In the top panels, for  $z = 0$  and  $z = 0.5$ , all ghost, generalised ghost and  $\Lambda$ CDM models generate the same number of objects at the low-mass end. However, at high masses, generalised ghost DE models with smaller value of the model parameter  $\gamma$  produce more objects. At higher redshifts,  $z = 1$  and  $z = 2$ ,



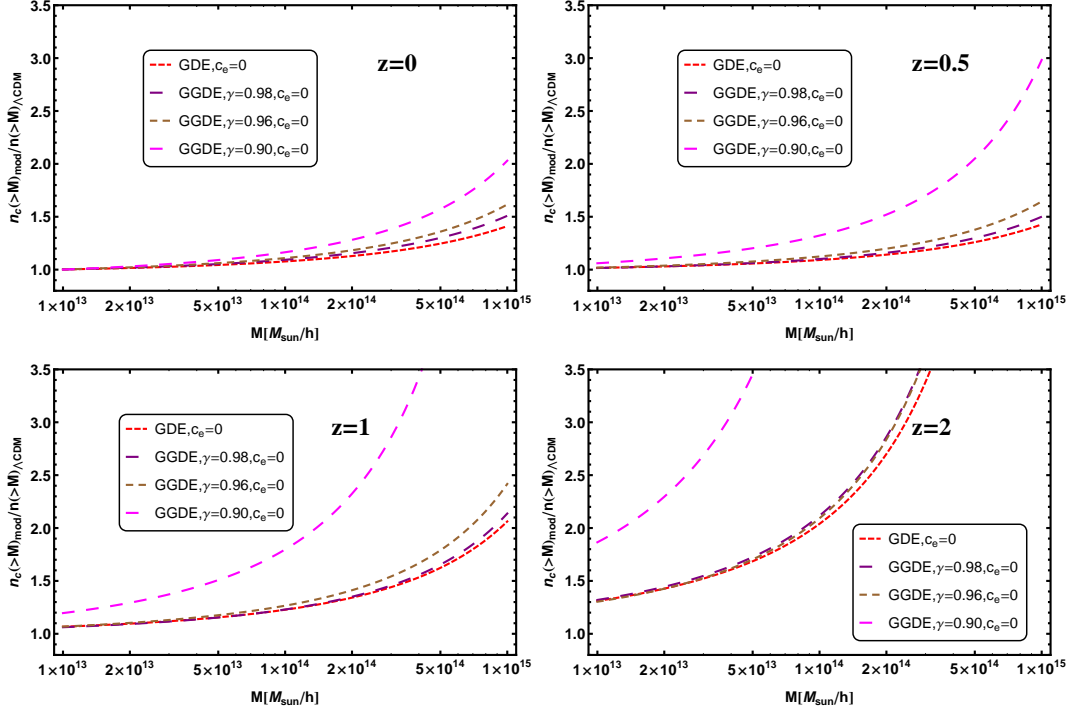


**Figure 7.** Ratio of the number of objects above a given mass  $M$  for halos at  $z = 0$  (top left panel),  $z = 0.5$  (top right panel),  $z = 1.0$  (bottom left panel) and  $z = 2.0$  (bottom right panel) between the ghost and generalised ghost DE models and the concordance  $\Lambda$ CDM model by using the mass definition in equation (32). The red dotted-dashed curve represents the clustering ghost DE model. The purple long dashed, brown dashed and pink long-dashed curves stand for clustering generalised ghost DE model with model parameter  $\gamma = 0.98$ ,  $\gamma = 0.96$  and  $\gamma = 0.90$ , respectively.

one can see that ghost and generalised ghost DE models have more objects for both the low mass and the high mass tail compared to the concordance  $\Lambda$ CDM model. Comparing figures (5) and (7), we conclude that for all the redshifts here considered, the predicted relative number density of halos in the presence of DE corrections to the halo mass is higher than what was found for homogeneous DE scenarios. In particular, the differences are larger for high-mass objects. This feature of ghost and generalised ghost DE models is in agreement with the results of Batista & Pace (2013) for inhomogeneous Early Dark Energy models. To compare the models quantitatively, we restrict our analysis to  $z = 0$ . While non-clustering DE models and the  $\Lambda$ CDM model have the same number of objects (top-left panel of figure (5)), clustering DE models deviate from the  $\Lambda$ CDM model particularly at the high-mass tail (top-left panel of figure (7)). We see that clustering generalised ghost DE model with  $\gamma = 0.90$  doubles the values obtained for the  $\Lambda$ CDM model, while for  $\gamma = 0.96$  the increment in the number of objects is  $\approx 61\%$ . Finally, for  $\gamma = 0.98$ , differences are of the order of 50%. As expected, the increase in  $\gamma$  corresponds to a decrease in the differences with respect to the  $\Lambda$ CDM model at the high mass tail (of the order of 40% for the ghost dark energy model).

## 5 CONCLUSIONS

In this work we studied the non-linear evolution of structure formation in ghost and generalised ghost dark energy models within the framework of the spherical collapse model. Dark energy models are described by a constant or a time varying equation of state  $w(a)$  whose functional form is usually purely phenomenological.

The advantage of dynamical dark energy models with respect to the  $\Lambda$ CDM model is that to alleviate its theoretical problems. Another interesting aspect is the presence of fluctuations in the dark energy fluid that can have an important and characteristic impact on non-linear structure formation. Ghost dark energy models are theoretically well motivated and trace their origin back to the studies of the low energy effective QCD theory (Veneziano 1979; Witten 1979; Kawarabayashi & Ohta 1980; Rosenzweig et al. 1980). Here we concentrate on the cosmological implications of such models and present results that can be useful from an observational point of view.

We start our analysis by studying the effects of the modification of the background expansion history of the growth factor and on a second step we take into account also the perturbations in the dark energy component. We showed that the linear growth factor is sensitive to the details of the model considered. In particular, when dark energy is homogeneous, differences with respect to the  $\Lambda$ CDM model are very pronounced and can be up to 50% at relatively high redshifts. Interestingly, when dark energy fluctuations are taken into account, differences become smaller and the models studied get closer to the  $\Lambda$ CDM model. This is exactly what happens for early dark energy model and it applies to this class of models as well, being the amount of dark energy at early times significantly more important (see bottom panel of figure (1)).

Being the equations governing the evolution of the linearly extrapolated overdensity parameter  $\delta_c$  identical to those of the linear growth factor, results are similar to what found for the linear growth factor. Once again when the perturbations in the dark energy fluid are included in the calculations, the models examined resemble closer the  $\Lambda$ CDM model. This is easily explained by tak-

ing into account that when dark energy perturbations play a role, Poisson equation is modified and this makes the model more similar to the  $\Lambda$ CDM one (see Batista & Pace 2013, for a more detailed discussion). Similar conclusions can be drawn for the non-linear virial overdensity  $\Delta_V$ .

While the growth factor can be inferred from the determination of the matter power spectrum on linear scales at a given redshift or by measuring the quantity  $f\sigma_8(z)$ , where  $f = d\ln D_+/d\ln a$  and  $\sigma_8(z) = D_+(z)\sigma_8(z=0)$ , the linear extrapolated overdensity  $\delta_c$  is a purely theoretical quantity and it would be very hard to infer it from observations. Nevertheless they can be combined together and be the basic ingredients to evaluate the mass function and the number of halos above a given mass. When keeping the dark energy fluid smooth and important only at the background level, we showed that both the ghost and generalised ghost models give an excess of objects with respect to the  $\Lambda$ CDM model, except for the generalised ghost model with lower value  $\gamma = 0.9$ . As expected, differences are very pronounced only for the high mass tail of the mass function, while at low masses the models are practically indistinguishable.

One might consider that if dark energy can clump, then the total mass of the halos should be affected. By defining the contribution of dark energy limited to that of the clumps, we showed in the top panel of figure (6) that the dark energy mass can be at least 10% of the dark matter mass at  $z = 0$ , with differences growing with decreasing the parameter  $\gamma$  and decreasing at high redshift where the contribution of dark energy is less important. Note that if the amount of dark energy at early times is significantly bigger than in the  $\Lambda$ CDM model, then the dark energy mass can still be an appreciable fraction of the dark matter mass. By taking into account this correction and evaluating the number of objects above a given mass, we showed that the dark energy models we studied in this work predict much more objects with respect to the  $\Lambda$ CDM model at all redshifts. This could be a good test to compare theoretical predictions with observations.

## References

- Abramo L. R., Batista R. C., Liberato L., Rosenfeld R., 2007, *Journal of Cosmology and Astro-Particle Physics*, 11, 12
- Abramo L. R., Batista R. C., Liberato L., Rosenfeld R., 2008, *Phys. Rev. D*, 77, 067301
- Abramo L. R., Batista R. C., Liberato L., Rosenfeld R., 2009, *Phys. Rev. D*, 79, 023516
- Abramo L. R., Batista R. C., Rosenfeld R., 2009, *J. Cosmol. Astropart. Phys.*, 7, 40
- Ade P. A. R., Aghanim N., Armitage-Caplan C., Arnaud M., Ashdown M., Atrio-Barandela F., Aumont J., Baccigalupi C., Banday A. J., et al. 2013a, *ArXiv e-prints*, 1303.5079
- Ade P. A. R., Aghanim N., Armitage-Caplan C., Arnaud M., Ashdown M., Atrio-Barandela F., Aumont J., Baccigalupi C., Banday A. J., et al. 2013b, *ArXiv e-prints*, 1303.5080
- Appleby S. A., Linder E. V., Weller J., 2013, *Phys. Rev. D*, 88, 043526
- Arkani-Hamed N., Creminelli P., Mukohyama S., Zaldarriaga M., 2004, *J. Cosmol. Astropart. Phys.*, 04, 001
- Armendariz-Picon C., Mukhanov V., Steinhardt P. J., 2001, *Phys. Rev. D*, 63(10), 103510
- Ascasibar Y., Yepes G., Gottlöber S., Müller V., 2004, *MNRAS*, 352, 1109
- Avila-Reese V., Firmani C., Hernández X., 1998, *ApJ*, 505, 37
- Barkana R., Loeb A., 2001, *Phys. Rep.*, 349, 125
- Basse T., Bjælde O. E., Wong Y. Y., 2011, *JCAP*, 10, 38
- Batista R. C., Pace F., 2013, *JCAP*, 6, 44
- Bertschinger E., 1985, *ApJS*, 58, 39
- Bond J. R., Cole S., Efstathiou G., Kaiser N., 1991, *ApJ*, 379, 440
- Bromm V., Yoshida N., 2011, *ARA&A*, 49, 373
- Cai R. G., 2007, *Phys. Lett. B*, 657, 228
- Cai R. G., Tuo Z. L., Wu Y. B., Zhao Y. Y., 2012, *Phys. Lett. B*, 86, 023511
- Cai R. G., Tuo Z. L., Zhang H. B., Su Q., 2011, *Phys. Rev. D*, 84, 123501
- Caldwell R. R., 2002, *Phys. Lett. B*, 545, 23
- Carroll S. M., 2001, *Living Reviews in Relativity*, 380, 1
- Chiba T., Okabe T., Yamaguchi M., 2000, *Phys. Rev. D*, 62, 023511
- Ciardi B., Ferrara A., 2005, *Space Science Reviews*, 116, 625
- Copeland E. J., Sami M., Tsujikawa S., 2006, *International Journal of Modern Physics D*, 15, 1753
- Creminelli P., DŠAmico G., NoreŸna J., Senatore L., Vernizzi F., 2010, *JCAP*, 3, 27
- del Popolo A., Pace F., Lima J. A. S., 2013a, *International Journal of Modern Physics D*, 22, 1350038
- del Popolo A., Pace F., Lima J. A. S., 2013b, *MNRAS*, 430, 628
- del Popolo A., Pace F., Lima J. A. S., 2013c, *Phys. Rev. D*, 87, 043527
- Eisenstein D. J., Zehavi I., Hogg D. W., Scoccimarro R., Blanton M. R., Nichol R. C., Scranton R., Tegmark M., Zheng Z., et al. 2005, *ApJ*, 633, 560
- Fillmore J. A., Goldreich P., 1984, *ApJ*, 281, 1
- Gasperini M., Veneziano F. P. G., 2002, *Phys. Rev. D*, 65, 023508
- Gunn J. E., Gott J. R., 1972, *ApJ*, 176, 1
- H. Guth A., 1981, *Phys. Rev. D*, 23, 347
- Ho S., Hirata C., Padmanabhan N., Seljak U., Bahcall N., 2008, *Phys. Rev. D*, 78, 043519
- Hoffman Y., Shaham J., 1985, *ApJ*, 297, 16
- Hořava P., Minic D., 2000, *Physical Review Letters*, 85, 1610
- Horellou C., Berge J., 2005, *MNRAS*, 360, 1393
- Jaffe A. H., Ade P. A., Balbi A., Bock J. J., Bond J. R., Borrill J., Boscaleri A., et al. 2001, *Physical Review Letters*, 86, 3475
- Jarosik N., Bennett C. L., Dunkley J., Gold B., Greason M. R., Halpern M., Hill R. S., Hinshaw G., Kogut A., Komatsu E., et al. 2011, *ApJS*, 192, 14
- Kawarabayashi K., Ohta N., 1980, *Nucl. Phys. B*, 175, 477
- Komatsu E., Smith K. M., Dunkley J., et al. 2011, *ApJS*, 192, 18
- Lahav O., Lilje P. B., Primack J. R., Rees M. J., 1991, *MNRAS*, 251, 128
- Linde A., 1990, *Physics Letters B*, 238, 160
- Maggiore M., Hollenstein L., Jaccard M., Mitsou E., 2012, *Phys. Lett. B*, 704, 102
- Maor I., Lahav O., 2005, *JCAP*, 7, 3
- Mehrabi A., Malekjani M., Pace F., 2014, *Astrophys Space Sci*, 355, 2185
- Mota D. F., van de Bruck C., 2004, *A&A*, 421, 71
- Naderi T., Malekjani M., Pace F., 2015, *MNRAS*, 447, 1873
- Nojiri S., Odintsov S. D., 2003a, *Phys. Lett. B*, 562, 147
- Nojiri S., Odintsov S. D., 2003b, *Phys. Lett. B*, 565, 1
- Ohta N., 2011, *Phys. Lett. B*, 695, 41
- Pace F., Batista R. C., Popolo A. D., 2014, *MNRAS*, 445, 648
- Pace F., Fedeli C., Moscardini L., Bartelmann M., 2012, *MNRAS*, 422, 1186
- Pace F., Moscardini L., Crittenden R., Bartelmann M., Pettorino V., 2014, *MNRAS*, 437, 547
- Pace F., Waizmann J. C., Bartelmann M., 2010, *MNRAS*, 406, 1865
- Padmanabhan T., 2002, *Phys. Rev. D*, 66, 021301
- Padmanabhan T., 2003, *Phys. Rep.*, 380, 235
- Peacock J. A., 1999, *Cosmological Physics*. Cambridge University Press
- Peebles P. J., Ratra B., 2003, *Reviews of Modern Physics*, 75, 559
- Peebles P. J. E., 1993, *Principles of physical cosmology*. Princeton University Press
- Percival W. J., Reid B. A., Eisenstein D. J., et al. 2010, *MNRAS*, 401, 2148
- Perlmutter S., Aldering G., Goldhaber G., et al. 1999, *ApJ*, 517, 565
- Piazza F., Tsujikawa S., 2004, *J. Cosmol. Astropart. Phys.*, 07, 004
- Press W. H., Schechter P., 1974, *ApJ*, 187, 425
- Riess A. G., Filippenko A. V., Challis P., et al. 1998, *AJ*, 116, 1009
- Riess A. G., Strolger L. G., Casertano S., Ferguson H. C., Mobasher B., Gold B., Challis P. J., et al. 2007, *ApJ*, 659, 98

- Riess A. G., Strolger L. G., Tonry J., Casertano S., Ferguson H. C., et al. 2004, *ApJ*, 607, 665
- Rosenzweig C., Schechter J., Trahern C., 1980, *Phys. Rev. D*, 21, 3388
- Ryden B. S., Gunn J. E., 1987, *ApJ*, 318, 15
- Sahni V., Starobinsky A., 2000, *International Journal of Modern Physics D*, 9, 373
- Sen A., 2002, *J. High Energy Phys.*, 04, 048
- Sheth R. K., Tormen G., 1999, *MNRAS*, 308, 119
- Sheth R. K., Tormen G., 2002, *MNRAS*, 329, 61
- Starobinsky A. A., 1980, *Physics Letters B*, 91, 99
- Subramanian K., Cen R., Ostriker J. P., 2000, *ApJ*, 538, 528
- Tegmark M., Strauss M. A., Blanton M. R., Abazajian K., Dodelson S., Sandvik H., Wang X., Weinberg D. H., Zehavi I., Bahcall N. A., et al. 2004, *Phys. Rev. D*, 69, 103501
- Thomas S., 2002, *Physical Review Letters*, 89, 081301
- Urban F., Zhitnitsky A., 2009a, *Phys. Rev. D*, 80, 063001
- Urban F., Zhitnitsky A., 2009b, *J. Cosmol. Astropart. Phys.*, 0909, 018
- Urban F., Zhitnitsky A., 2010a, *Phys. Lett. B*, 688, 9
- Urban F., Zhitnitsky A., 2010b, *Nucl. Phys. B*, 835, 135
- Veneziano G., 1979, *Nucl.Phys. B*, 159, 213
- Wang L., Steinhardt P. J., 1998, *ApJ*, 508, 483
- Wang Y., Tegmark M., 2005, *Phys. Rev. D*, 71, 103513
- Weinberg S., 1989, *Reviews of Modern Physics*, 61, 1
- Wetterich C., 1988, *Nucl. Phys. B*, 302, 668
- White S. D. M., Rees M. J., 1978, *MNRAS*, 183, 341
- Williams L. L. R., Babul A., Dalcanton J. J., 2004, *ApJ*, 604, 18
- Witten E., 1979, *Nucl.Phys. B*, 156, 269
- Zhitnitsky A. R., 2011, *Phys. Rev. D*, 84, 124008

This paper has been typeset from a  $\text{\LaTeX}$  file prepared by the author.